View Online / Journal Homepage / Table of Contents for this issue
Dynamic Article Links

Soft Matter

Cite this: *Soft Matter*, 2011, **7**, 11154

www.rsc.org/softmatter

PAPER

Liquid crystals of aqueous, giant graphene oxide flakes†

Budhadipta Dan,[ad] Natnael Behabtu,[b] Angel Martinez,[d] Julian S. Evans,[d] Dmitry V. Kosynkin,[c] James M. Tour,[c] Matteo Pasquali*[bc] and Ivan I. Smalyukh*[def]

Received 25th July 2011, Accepted 19th September 2011
DOI: 10.1039/c1sm06418e

We report the observation of liquid crystals formed by giant graphene oxide flakes (aspect ratio above 10 000) suspended in water. As their concentration increases, the flakes undergo transitions from an isotropic dispersion to a biphasic system and then to a discotic nematic liquid crystal. The gel-like liquid crystal displays an unusual defect-free uniform director alignment over hundreds of micrometres. We characterize the nematic order parameter, optical birefringence and elastic properties of this novel mesomorphic system.

Colloidal suspensions of anisotropic particles have been the subject of continued research for over 100 years, owing to their rich variety of liquid crystalline phases and fascinating phase transitions.[1] Initial studies on the orientational ordering, optical, and elastic properties of liquid crystals (LCs) were performed primarily on suspensions of rod-like particles.[2–5] Onsager[4] noted that liquid crystallinity is not restricted to only rod-like building blocks, but should also extend to other anisotropic shapes, like disks and platelets. Experimental realization of disk and platelet LC systems, however, was achieved much later[6] and has been a topic of intense research since that time.[7,8] In the mid 1960s, mesophases of disk-like molecules were observed during the high temperature carbonization of graphitizable substances such as petroleum and coal tar pitches.[9] Their complex, polydisperse composition, consisting of multi-component polyaromatic molecules, likely impeded a detailed investigation of this naturally occurring "carbonaceous mesophase". The first experimental observation of discotic mesophase in a pure, single-component organic molecule system was reported in 1977 by Chandrasekhar *et al.*[6] They prepared a number of benzene-hexa-*n*-alkanoates, compounds with rigid aromatic cores and flexible aliphatic side chains, and used optical and X-ray studies to unambiguously demonstrate the existence of discotic LCs.

During the last three decades, more than 50 different organic cores and 3000 derivatives have been shown forming discotic LCs.[8] Most molecules are a single atomic layer thick (thickness $h < 1$ nm) and a few nanometres in diameter (D), *i.e.*, of typical aspect ratios $D/h \sim 5$. A majority of these aromatic-core based compounds demonstrate columnar discotic LC phases, where strong π–π interactions allow the disk-like molecules to assemble into cylindrical structures which in turn act as mesogens. A nematic mesophase, which is the prevalent mesophase observed in calamitic molecules, is not common among discotic organic molecules.[10] Lyotropic LC phases have been observed in colloidal dispersions of inorganic platelets.[11–13] Isotropic to discotic nematic, and columnar LC phase transitions have been reported in dispersions of several systems including nickel hydroxide,[14] gibbsite[15,16] and layered double hydroxide.[17,18] The mineral platelets are typically larger in size ($D \sim$ hundreds of nanometres). However, an accompanying higher thickness often limits the highest achievable aspect ratio to only $D/h \sim 20$.

Recently, Behabtu *et al.*[19] reported the liquid crystallinity of graphene suspensions in chlorosulfonic acid at high graphene concentration (2 wt%). While the present work was under preparation and submission, Kim *et al.*[20] and Xu and Gao[21] reported discotic nematic fluid behavior in aqueous suspensions of graphene oxide, qualitatively similar to graphene in strong acids.[19] In this work, we explore the lyotropic phase behavior of high aspect ratio ($D/h \sim 10^4$ and higher) giant graphene oxide (GGO) flakes in aqueous suspension; discotic building blocks with the highest aspect ratio and largest lateral dimensions to our knowledge and an order of magnitude higher than the previous reports. We demonstrate that higher aspect ratio leads to a dramatic change in the mesomorphic behavior; GGO dispersions form gel-like liquid crystals instead of fully fluid nematics reported previously for both graphene[19] and graphene oxide[20,21] and mesomorphic behavior is observed at concentrations an

[a]*Department of Physics and Astronomy, 6100 Main Street, Houston, Texas, 77005, USA*
[b]*Department of Chemical and Biomolecular Engineering, 6100 Main Street, Houston, Texas, 77005, USA. E-mail: mp@rice.edu*
[c]*Department of Chemistry, R. E. Smalley Institute for Nanoscale Science & Technology, Rice University, 6100 Main Street, Houston, Texas, 77005, USA*
[d]*Department of Physics, 2000 Colorado Ave, Boulder, Colorado, 80309, USA. E-mail: ivan.smalyukh@colorado.edu*
[e]*Materials Science and Engineering Graduate Program, and Liquid Crystal Materials Research Center, University of Colorado, 2000 Colorado Ave, Boulder, Colorado, 80309, USA*
[f]*Renewable and Sustainable Energy Institute, University of Colorado and National Renewable Energy Laboratory, Boulder, Colorado, 80309, USA*
† Electronic supplementary information (ESI) available: Additional SEM images of GGO flakes. See DOI: 10.1039/c1sm06418e

order of magnitude lower than what has been achieved for discotic mesogens. Optical methods are used to reveal the alignment of GGO flakes in the ordered phase, and measure the birefringence and order parameter; scaling law provides an estimate for the Frank elastic constant of this novel discotic LC system. Controlled confinement and colloidal inclusions are employed to induce LC defects and elastic distortions in the GGO director field.

Much like in the case of polymers and single wall carbon nanotubes (SWNTs), the liquid crystalline phase of graphene and graphene oxide is an important precursor for fabrication of high performance multifunctional aligned fibers. Discotic LCs of graphitic hydrocarbons are also attractive for applications in advanced electronics.[22] Both mechanical and electrical properties of such graphene based macrostructures are expected to improve with increasing aspect ratio of individual molecules; similar scaling has already been demonstrated for the structurally similar SWNTs.[23] Therefore, LC suspensions of high aspect ratio graphene are of strong practical interest. From a fundamental point of view, these systems could be the closest experimental realization of theoretical models based on infinitely thin and high aspect ratio rigid platelets.[24,25]

The GGO flakes were prepared by the method of Ref. 26 These monolayer GGO flakes tend to have a more regular structure and larger continuous regions of intact basal plane, compared to graphene oxide produced using other conventional techniques like Hummer's method.[27] The presence of functional groups such as epoxy, hydroxyls, carbonyls, and carboxylates render the flakes hydrophilic. The average size and polydispersity of GGO flakes was characterized using transmission electron microscopy (TEM) and scanning electron microscopy (SEM), as shown in Fig. 1. The GGO flakes had irregular polygonal shapes with a few ribbon-like structures (additional images in supplementary information†). They had a number-average equivalent diameter $\langle d \rangle$ of 12 μm with relative standard deviation $\sigma_d = (\langle d^2 \rangle - \langle d \rangle^2)^{1/2} / \langle d \rangle$ of 59%. The median aspect ratio of flakes was 10^4; in comparison, aspect ratio of graphene and graphene oxide in previous reports were: Behabtu *et al.* ~ 700, Kim *et al.* ~ 1200 and Xu and Gao ~ 2600.

The phase behavior of aqueous suspensions of GGO flakes was investigated for a concentration range of 0.01–0.14 vol%.

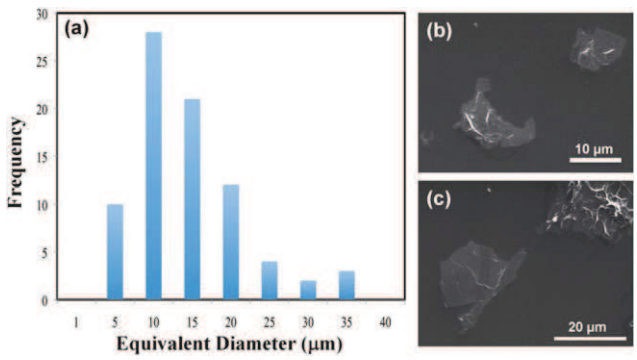

Fig. 1 (a) Size distribution of monolayer GGO flakes obtained through SEM and TEM imaging. (b,c) Representative SEM images of flakes prepared by spin coating dilute aqueous GGO suspension on silicon substrates.

Drops from suspensions with different GGO concentrations were squeezed between a cover slip and a glass slide whose edges were sealed with epoxy glue. These samples were examined using a bright field transmission-mode optical polarizing microscope (Olympus BX51) with 50x and 100x oil immersion objectives and between crossed-polarizers. The dilute suspensions (< 0.05 vol%; assuming density of GGO ~ 2000 kg m^{-3})[28] appeared dark and featureless under crossed-polarizers, as shown in Fig. 2(a). Lack of visible aggregates indicated a stable suspension. Suspensions with GGO concentration above ~ 0.05 vol% displayed regions with weak birefringence, indicating onset of ordering and a biphasic system, Fig. 2(b). The fraction of ordered phase in the sample, as detected under crossed-polarizers, increased with GGO concentration. Above ~ 0.1 vol%, the entire sample appeared birefringent at different stages of sample rotation under crossed-polarizers, indicating a single-phase LC state, Fig. 2(c). Our observations are consistent with theoretical predictions for a colloidal system comprised of infinitely thin and monodisperse disk-like particles, which is expected to transition from isotropic to nematic at a volume fraction of $\Phi_{iso} = 4\ h/D$.[24] Φ_{iso} = 0.04 vol% for GGO flakes, in good agreement with the experiments (Fig. 2(a-d)). The existence of a rather wide biphasic region (0.05–0.1 vol%) can be partially attributed to the polydispersity in flake size, although even monodisperse flakes can exhibit biphasic behavior.

The high-concentration GGO suspensions had a gel-like consistency (Fig. 2(c)). Gelation has been observed previously in several other lyotropic discotic LC systems; most notably clay, whereby upon increasing the concentration, suspensions transition from an isotropic liquid to an isotropic gel to a birefringent gel.[29–31] Uniformly aligned nematic domains of GGO were prepared by dipping one end of a rectangular glass capillary tube (50 μm thick and 0.5 mm wide, inner dimensions, obtained from Vitrocom) in dilute isotropic GGO suspension (~0.03 vol%), causing spontaneous filling due to capillary action. Subsequent slow evaporation of water through the capillary ends led to

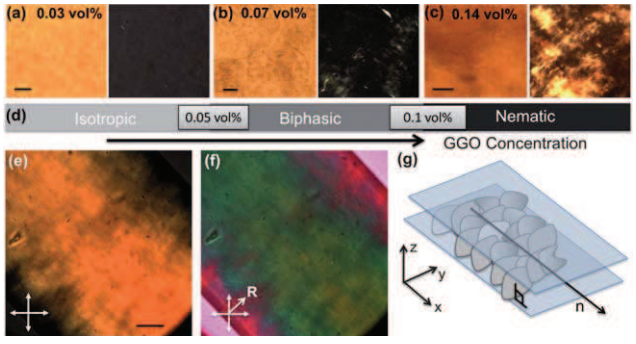

Fig. 2 (a–c) Optical microscopy images obtained without analyzer (left) and between crossed-polarizers (right) of GGO aqueous suspensions, demonstrating phase behavior *vs.* concentration: (a) isotropic (0.03 vol %), (b) biphasic (0.07 vol%) and (c) nematic (0.14 vol%). The scale bar in (a–c) is 10 μm. (d) Phase behavior *vs.* concentration. (e,f) Polarizing microscopy images of GGO nematic phase, inside a capillary, obtained with and without retardation plate, respectively; uniform birefringence indicates uniform alignment of director over large length scales. The scale bar in (e) is 20 μm and "R" in (f) marks the slow axis of phase retardation plate. (g) Schematic showing the alignment of flakes.

a continuous increase of concentration of GGO flakes in the suspension. Upon observation of birefringent textures, the tube ends were sealed with epoxy glue to prevent further drying. Fig. 2 (e) shows an optical micrograph under crossed polarizers of a high concentration GGO suspension prepared using this procedure. Uniform brightness across the entire field of view indicates a well-aligned director (***n***) over large length scales (hundreds of microns or more). Moreover, it indicates that the GGO flakes are oriented perpendicular to the wide top and bottom sides of the rectangular capillary (since flakes parallel to the top and bottom sides of the capillary would not produce birefringent textures). It is important to note that the observed flake alignment with respect to the top and bottom sides of capillary is likely metastable as it is partly driven by the kinetics of sample preparation procedure. The kinetics of the sample preparation process likely aids in the uniform director alignment as well, in addition to the intrinsic elasticity of the sample which is discussed in further details later.

The direction of in-plane orientation for GGO flakes was determined by inserting a full wave retardation plate (530 nm), also called "red plate", between the sample and analyzer, with its slow axis oriented at 45° with respect to the polarizer. For a GGO flake, the axis along the basal plane represents slow axis while the normal to plane is the fast axis. Therefore, the appearance of bluish-green color (Fig. 2(f)), which in the case of GGO flakes (with negative birefringence) indicates addition of phase retardations of the sample and the red plate,[32] shows that the GGO flakes are also oriented normal to the length of the capillary. The above analysis yields the overall arrangement and orientation of GGO flakes and the nematic director in the LC phase shown in Fig. 2(g).

Remarkably, uniform director orientation over ~1 mm length scales was achieved without any surface alignment layer, such as is typically required for small molecule LCs; this likely indicates high elastic constant values. Indeed, according to density functional theory based models for nematic discotic systems, the average Frank elastic constant (K) of a nematogen can be expressed as:[33]

$$K \propto Q^{2/3}(Q^{-2} + 2)S^2 \quad (1)$$

where $Q = D/h$ is the aspect ratio of nematogens and S is the nematic scalar order parameter. For disk-shaped nematogens, $Q \gg 1$ and the average elastic constant scales as $K \propto Q^{2/3}$. Previous studies on discotic nematics with average aspect ratios of $Q \sim 5$ have reported average elastic constants on the order of 1 pN.[34–36] Because the elasticity coefficients of nematogens are mainly sensitive to the average molecular dimensions,[33] the average elastic constant of GGO ($Q \sim 10^4$) was estimated to be $K_{GGO} \sim$ 100 pN, at least one order of magnitude higher than that of most previously studied discotic nematics.

The highly uniform samples prepared in rectangular capillaries enabled characterization of the GGO LC parameters, such as the optical birefringence (Δn) and the order parameter (S). The optical birefringence was measured by use of a Berek compensator. Measurements were performed at several different locations, giving an average birefringence of $\Delta n = -0.0017 \pm 0.0005$ for the GGO LC. For comparison, the absolute values of birefringence of other discotic nematics are much larger, typically, −0.05 for polyacrylates[37] and −0.02 for disodium cromoglycate and −0.01 for violet-20 chromonic LC.[38] The order parameter of GGO flakes in the nematic phase was estimated using optical absorption anisotropy, as described in Ref.38. Liquid crystalline GGO in a 50 μm thick capillary was placed on a microscope stage between *parallel* polarizers, and illuminated with monochromatic green light. The transmittance through the sample was measured for director orientations of 0°, 45°, and 90° with respect to the polarizers (referred to as t_0, t_{45} and t_{90}, respectively). Corresponding absorption indices, k_0, k_{45} and k_{90}, were obtained from the expression

$$t_i = \exp(-4\pi k_i d/\lambda),$$

where $i = 0$, 45, 90 is indexed corresponding to director orientations of 0°, 45°, and 90°, respectively, at $\lambda = 550$ nm and $d = 50$ μm. For an ordered phase of disk-like molecules with the molecular planes oriented perpendicular to the director, if the shape of absorption spectrum is independent of molecular orientation and the birefringence is small (both conditions hold true for GGO), the scalar order parameter can be expressed as:[38]

$$S = \frac{1 - \Delta}{1 + \Delta/2} \quad (2)$$

where $\Delta = k_0/k_{90}$ is the linear dichroic ratio. The above expression evaluated at several different locations along the sample yields an average $S = 0.43 \pm 0.15$, which is lower than what has been measured for other discotic nematic LCs. In comparison, typical order parameter values measured in other LCs include ~ 0.9 for hexa-n-hexyloxytriphenylene,[7] 0.6–0.85 for 2,3,7,8,12,13-hexa-n-decanoyloxytruxene (H10TX) and 2,3,6,7,10,11-hexa-n-pentyloxytriphenylene (H5T),[39] and 0.8 for gibbsite particles.[40]

Optical absorption anisotropy provides an independent estimate of the birefringence. The phase retardation of transmitted light traversing an anisotropic sample is:[38]

$$\Delta\varphi = \cos^{-1}\left(\frac{4t_{45} - (t_0 + t_{90})}{2\sqrt{t_0 t_{90}}}\right) \quad (3)$$

The phase retardation is related to optical birefringence as $\Delta n = \Delta\varphi \cdot \lambda/2\pi d$. Calculations using this method yield an optical birefringence of $\Delta n = -0.0018 \pm 0.0009$, in good agreement with the value obtained *via* Berek compensator measurements.

Dispersion of colloidal particles in various types of LCs has been widely used for enhancement of LC properties, assembly of anisotropic structures, and alignment of anisotropic particles such as rods and discs.[41–49] We use anisotropic colloidal inclusions for direct visualization of orientation of GGO flakes in the nematic phase. Two types of particles were chosen for this purpose: gold microtriangles, 5 nm in thickness and up to 10 μm in side length, (Fig. 3(a)) prepared using a biosynthesis technique,[50] and glass micro-rods, 3 μm diameter and 10 μm long (from Duke Scientific). Gold triangular platelets spontaneously oriented inside the GGO nematic phase with their large-area faces perpendicular to ***n*** and parallel to GGO flakes, as shown in Fig. 3(b-c), and consistent with cross-polarized optical images. Glass micro-rods spontaneously aligned with their long axes perpendicular to ***n*** and parallel to the GGO flakes, as shown in Fig. 3(d,e,f). The ability of GGO LC to disperse and align anisotropic colloidal particles is important from an applications

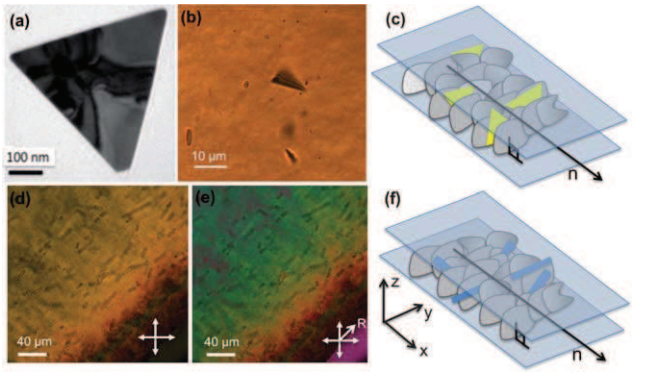

Fig. 3 Anisotropic colloidal particles and their spontaneous alignment in GGO nematic LC. (a) TEM image of an anisotropic gold triangular platelet. (b) Bright-field transmission-mode image showing triangular platelets with up to 10 μm side length and 5 nm thickness as they spontaneously align parallel to GGO flakes of the LC. (c) Schematic diagram of the GGO flake and gold platelet alignment. (d–e) Polarizing microscopy images showing spontaneous alignment of glass micro-rods in the GGO LC observed under crossed polarizers with (d) and without (e) an additional retardation plate. (f) Schematic showing the alignment of micro-rods in the LC.

perspective. For example, the large scale ordering and alignment of anisotropic plasmonic nanoparticles such as gold, silver and palladium nanorods by means of dispersion in a LC is a valuable route for development of optoelectronic devices and metamaterials.[49]

Given the natural propensity of our GGO flakes to form large LC domains with uniform $\boldsymbol{n}$, the samples rarely exhibited defects. In order to induce defects, drops of dilute GGO suspension with circular footprints were trapped between a glass slide and cover slip, separated by 60 μm spacers and evaporated slowly to achieve a nematic phase. The recession of meniscus from all directions forces the formation of a defect at the center of drop. Interestingly, in most cases, the circular drops transformed into roughly Y-shaped structures as the drop radii became sufficiently small, likely due to the high elastic constant of GGO nematogens. The optical transmission image of an $s = -1/2$ defect, observed at the center of such Y-shaped nematic structures, is shown in Fig. 4(a). The arrangement of GGO flakes and director field around the defect is shown schematically in Fig. 4(b). Fig. 4 (c-d) show the polarizing optical micrographs of the defect structure with crossed-polarizers in 0°–90° and at 45°–135° orientations, respectively; the orientation of two dark brushes parallel to one of the polarizers is consistent with the schematically shown model of the defect structure.

Elastic distortions and defects in LCs can be also induced by inclusion of colloidal particles. Colloidal spheres suspended in nematics lead to particle-size dependent dipolar and quadrupolar distortions in the surrounding director field.[42–48] Minimization of the ensuing elastic energy due to distortions induced by these inclusions often results in spontaneous assembly of colloidal particles into anisotropic colloidal structures. In our study, we used melamine resin colloidal microspheres with diameters ranging from 2 μm to 15 μm. Aqueous microspheres (< 1 vol%) were mixed in the dilute GGO suspension, followed by capillary filling and solvent evaporation. Interestingly, small diameter

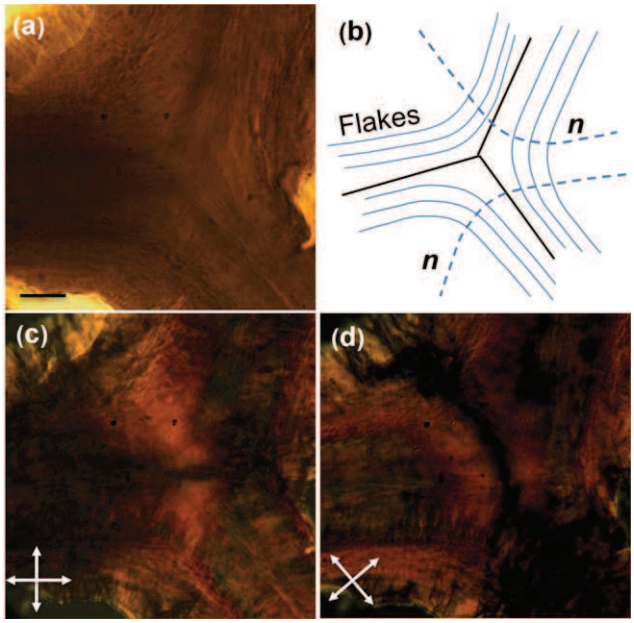

Fig. 4 A half-integer s= −1/2 disclination in the director field of GGO LC observed when the nematic phase was attained by solvent evaporation under the confinement of a glass slide and cover slip. (a) Transmission-mode bright field image. (b) Schematic of the arrangement of GGO flakes, (c,d) Polarizing microscopy images of the same region obtained (c) between vertical and horizontal crossed polarizers and (d) with crossed-polarizers at 45° and 135° with respect to horizontal side of the image. The scale bar in (a) is 20 μm.

particles (≤ 3 μm) did not produce detectable distortions, Fig. 5 (a), while larger particles (4–15 μm) produced distinct distortions in the director field, Fig. 5(b-d). Optical analysis of these

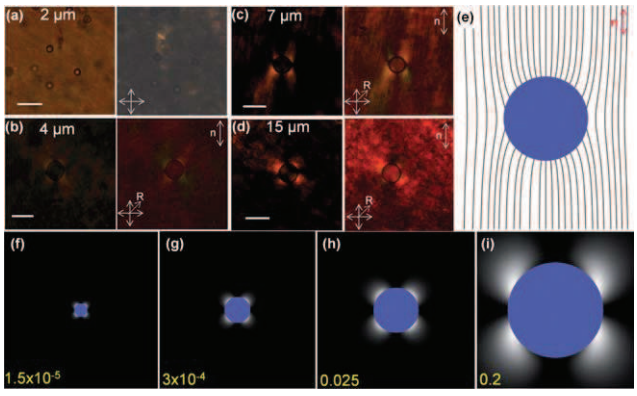

Fig. 5 Quadrupolar distortions in nematic director field around spherical inclusions, demonstrating homeotropic surface anchoring of the director. (a) Transmission-mode bright field (left) and between crossed polarizers (right) images of GGO LC. (b–d) Images of sample between crossed-polarizers (left) and with a retardation plate (right). Scale bars are 10 μm (a), 5 μm (b), 10 μm (c), 20 μm (d). Particle sizes, and orientations of crossed polarizers and retardation plates marked on the images. Computer-simulated (e) director field and (f–i) polarizing microscopy textures for particle sizes 2, 4, 7, and 15 μm, respectively. The values shown in (f–i) in yellow color are the ratios of maximum transmitted and incident light intensities for the corresponding computer-simulated images.

distortions using the "red plate" revealed "homeotropic" surface anchoring for $\boldsymbol{n}$, *i.e.* GGO flakes exhibit tangential alignment to the melamine resin particles. The orientation of GGO flakes around melamine resin particles is likely influenced by acid–base interactions between the $-NH_2$ and $=N-$ groups on melamine resin and acidic hydrophilic functional groups on GGO flakes.

The particle size-dependent distortions observed in GGO LC provide important insights into the interplay of bulk elastic and surface anchoring energies, which often determine whether a colloidal inclusion in a nematic LC will induce defects in the director field or barely perturb it.[41–48] For example, a spherical colloidal inclusion with homeotropic anchoring induces a pattern of director equivalent to that around a point defect with charge +1, known as a "radial hedgehog".[42] Therefore, the distortions around the particle, should be accompanied by a hyperbolic hedgehog or a half-integer "Saturn ring" disclination loop, (both having topological charge of −1) in order to conserve the total topological charge in the sample with a uniform far-field alignment.[42,47] On the other hand, nanoparticles of size only somewhat larger than that of the LC molecules and microparticles with weak surface anchoring typically produce either weak or no elastic distortions of the LC director field.[49] In the case of melamine resin particles suspended in GGO LC, no accompanying bulk or surface topological defects are observed (Fig. 4). The director distortions have quadrupolar symmetry, reminiscent of that formed around microparticles with weak homeotropic surface anchoring, suggesting that $K/W>R$, where R is particle radius and W is the polar surface anchoring coefficient.[42,48,49] Equivalently, the nematic director at the LC-colloid interface deviates from the "normal" orientation (Fig. 5(e)), in order to minimize elastic distortions and reduce the elastic energy at the expense of surface anchoring energy cost. The director distortions become less pronounced as R decreases, being barely noticeable for the 2 μm particles.

We have simulated the expected nematic director structure surrounding the particles and corresponding polarizing microscopy textures using the *ansatz* for LC director structure proposed by Ruhwandl and Terentjev[48] (Fig. 5(e)) and the Jones matrix method.[51] In the simulations, we have used estimated values of the elastic constant $K = 10^{-10}$ N, an optical anisotropy of $\Delta n = -0.0017$ and a polar anchoring coefficient of $W = 10^{-5}$ J m^{-2}, typical of lyotropic LCs.[49] The LC sample, with a colloidal inclusion and director distortions around it, was split into a set of thin slabs with known orientation of the optical axis ($\equiv \boldsymbol{n}$). In each pixel of a simulated polarizing microscopy texture (similar to those in Fig. 5(f-i)), intensity of the light after propagation through the cell was obtained by successive multiplication of the Jones matrices corresponding to a polarizer, the thin nematic slabs, and the analyzer. The computer simulated textures closely match the experimental results (Fig.5). Interestingly, although the particle diameters and the lateral GGO flake sizes are comparable, the director structures around the colloidal inclusions can still be understood based on simple considerations of the interplay between bulk elastic and surface anchoring energies originally developed for small-molecule LCs.

The melamine resin microspheres suspended in GGO LC are practically immobile and show no tendency to self-assemble into anisotropic structures, even at long time scales (several days), as has been reported in other nematic systems.[42–47] This is unexpected for anisotropic nematic fluids, given the distortions induced by the particles and the high elastic constant of GGO. The lack of particle motion and any noticeable interaction among the microspheres could be due to chemical interactions between the microspheres and flakes, a gel-like networked structure among the flakes and/or an extremely high viscosity at high GGO concentrations. Future studies are needed to decipher the nature of the forces responsible for the particle immobility.

In summary, we have shown that, with increasing concentration, aqueous suspensions of GGO flakes exhibit well-defined isotropic, biphasic and nematic LC behavior. Preparation of the nematic phase by slow evaporation of solvent from the isotropic phase yields large domains with uniform directors and minimal defects. Such large domains are consistent with estimated Frank elastic constant that is about one hundred-fold higher than in low-molecular-weight discotic nematics. Optical characterization yields a birefringence of $\Delta n \sim -0.0017$ and order parameter $S = 0.43$. We show that defects and elastic distortions can be deliberately induced by means of confinement and by colloidal inclusions. The studied spherical inclusions induce quadrupolar distortions of the director field and anisotropic particles self-align at a well-defined orientation with respect to the director and reveal the director structures. The liquid crystalline behavior from this new class of extremely high aspect ratio ($\sim 10^4$ and larger) disk-like building blocks could broadly impinge on both fundamental and applied aspects of discotic liquid crystals.

We acknowledge support of the Institute for Complex Adaptive Matter (ICAM), Colorado Renewable and Sustainable Energy Initiative, NSF grants DMR-0820579, DMR-0844115, and DMR-0847782, Air Force Research Lab grant FA 8650-07-2-5061 (managed by CONTACT), Air Force Office of Scientific Research grant FA9550-09-1-0590, Welch grant C-1668, U. S. Army Corps of Engineers Environmental Quality and Installation Program under grant W912HZ-08-C-0054, and M-I Swaco, LLC. The authors thank Dr. Bohdan Senyuk for assistance with the measurements of optical anisotropy and Prof. Noel Clark for discussions.

References

1 P. de Gennes and J. Prost, *The physics of liquid crystals*, Oxford University Press, USA, 1995.
2 H. Zocher, *Z. Anorg. Allg. Chem.*, 1925, **147**, 91–U15.
3 F. C. Bawden, N. W. Pirie, J. D. Bernal and I. Fankuchen, *Nature*, 1936, **138**, 1051–1052.
4 L. Onsager, *Ann. N. Y. Acad. Sci.*, 1949, **51**, 627–659.
5 G. J. Vroege and H. N. W. Lekkerkerker, *Rep. Prog. Phys.*, 1992, **55**, 1241–1309.
6 S. Chandrasekhar, B. K. Sadashiva and K. A. Suresh, *Pramana*, 1977, **9**, 471–480.
7 S. Chandrasekhar and G. S. Ranganath, *Rep. Prog. Phys.*, 1990, **53**, 57–84.
8 H. K. Bisoyi and S. Kumar, *Chem. Soc. Rev.*, 2010, **39**, 264–285.
9 J. D. Brooks and G. H. Taylor, *Nature*, 1965, **206**, 697–699.
10 D. A. Dunmur, *Physical Properties of Liquid Crystals: Nematics*, ed. D. A. Dunmur, A. Fukuda and G. R. Luckhurst, IEE, INSPEC, London, 2000.
11 F. M. van der Kooij, K. Kassapidou and H. N. W. Lekkerkerker, *Nature*, 2000, **406**, 868–871.
12 A. S. Sonin, *J. Mater. Chem.*, 1998, **8**, 2557–2574.
13 J. C. P. Gabriel and P. Davidson, *Adv. Mater.*, 2000, **12**, 9–20.
14 A. B. D. Brown, C. Ferrero, T. Narayanan and A. R. Rennie, *Eur. Phys. J. B*, 1999, **11**, 481–489.

15 F. M. van der Kooij and H. N. W. Lekkerkerker, *J. Phys. Chem. B*, 1998, **102**, 7829–7832.
16 D. van der Beek and H. N. W. Lekkerkerker, *Europhys. Lett.*, 2003, **61**, 702–707.
17 S. Y. Liu, J. Zhang, N. Wang, W. R. Liu, C. G. Zhang and D. J. Sun, *Chem. Mater.*, 2003, **15**, 3240–3241.
18 M. C. D. Mourad, E. J. Devid, M. M. van Schooneveld, C. Vonk and H. N. W. Lekkerkerker, *J. Phys. Chem. B*, 2008, **112**, 10142–10152.
19 N. Behabtu, J. R. Lomeda, M. J. Green, A. L. Higginbotham, A. Sinitskii, D. V. Kosynkin, D. Tsentalovich, A. N. G. Parra-Vasquez, J. Schmidt, E. Kesselman, Y. Cohen, Y. Talmon, J. M. Tour and M. Pasquali, *Nat. Nanotechnol.*, 2010, **5**, 406–411.
20 J. E. Kim, T. H. Han, S. H. Lee, J. Y. Kim, C. W. Ahn, J. M. Yun and S. O. Kim, *Angew. Chem., Int. Ed.*, 2011, **50**, 3043–3047.
21 Z. Xu and C. Gao, *ACS Nano*, 2011, **5**, 2908–2915.
22 L. Schmidt-Mende, A. Fechtenkotter, K. Mullen, E. Moons, R. H. Friend and J. D. MacKenzie, *Science*, 2001, **293**, 1119–1122.
23 N. Behabtu, M. J. Green and M. Pasquali, *Nano Today*, 2008, **3**, 24–34.
24 M. A. Bates and D. Frenkel, *J. Chem. Phys.*, 1999, **110**, 6553–6559.
25 R. Eppenga and D. Frenkel, *Mol. Phys.*, 1984, **52**, 1303–1334.
26 D. C. Marcano, D. V. Kosynkin, J. M. Berlin, A. Sinitskii, Z. Z. Sun, A. Slesarev, L. B. Alemany, W. Lu and J. M. Tour, *ACS Nano*, 2010, **4**, 4806–4814.
27 W. S. Hummers and R. E. Offeman, *J. Am. Chem. Soc.*, 1958, **80**, 1339–1339.
28 D. A. Dikin, S. Stankovich, E. J. Zimney, R. D. Piner, G. H. B. Dommett, G. Evmenenko, S. T. Nguyen and R. S. Ruoff, *Nature*, 2007, **448**, 457–460.
29 J. C. P. Gabriel, C. Sanchez and P. Davidson, *J. Phys. Chem.*, 1996, **100**, 11139–11143.
30 A. Mourchid, A. Delville, J. Lambard, E. Lecolier and P. Levitz, *Langmuir*, 1995, **11**, 1942–1950.
31 A. Mourchid, E. Lecolier, H. Van Damme and P. Levitz, *Langmuir*, 1998, **14**, 4718–4723.
32 E. E. Wahlstrom, *Optical crystallography*, John Wiley & Sons Inc., 1979.
33 M. A. Osipov and S. Hess, *Mol. Phys.*, 1993, **78**, 1191–1201.
34 B. Tjiptomargo, G. T. Evans, M. P. Allen and D. Frenkel, *J. Phys. Chem.*, 1992, **96**, 3942–3948.
35 T. Haven, D. Armitage and A. Saupe, *J. Chem. Phys.*, 1981, **75**, 352–364.
36 N. H. Phuong, G. Germano and F. Schmid, *J. Chem. Phys.*, 2001, **115**, 7227–7234.
37 C. D. FavreNicolin and J. Lub, *Macromolecules*, 1996, **29**, 6143–6149.
38 Y. A. Nastishin, H. Liu, T. Schneider, V. Nazarenko, R. Vasyuta, S. V. Shiyanovskii and O. D. Lavrentovich, *Phys. Rev. E: Stat., Nonlinear, Soft Matter Phys.*, 2005, **72**, 041711.
39 T. S. Perova and J. K. Vij, *Adv. Mater.*, 1995, **7**, 919–922.
40 D. van der Beek, P. Davidson, H. H. Wensink, G. J. Vroege and H. N. W. Lekkerkerker, *Phys. Rev. E: Stat., Nonlinear, Soft Matter Phys.*, 2008, **77**, 031708.
41 F. Brochard and P. G. D. Gennes, *J. Phys.*, 1970, **31**, 691.
42 P. Poulin, H. Stark, T. C. Lubensky and D. A. Weitz, *Science*, 1997, **275**, 1770–1773.
43 P. Poulin, N. Frances and O. Mondain-Monval, *Phys. Rev. E: Stat. Phys., Plasmas, Fluids, Relat. Interdiscip. Top.*, 1999, **59**, 4384–4387.
44 J. C. Loudet, P. Barois and P. Poulin, *Nature*, 2000, **407**, 611–613.
45 C. P. Lapointe, T. G. Mason and Smalyukh, II, *Science*, 2009, **326**, 1083–1086.
46 P. Poulin and D. A. Weitz, *Phys. Rev. E: Stat. Phys., Plasmas, Fluids, Relat. Interdiscip. Top.*, 1998, **57**, 626–637.
47 Smalyukh, II, A. V. Kachynski, A. N. Kuzmin and P. N. Prasad, *Proc. Natl. Acad. Sci. U. S. A.*, 2006, **103**, 18048–18053.
48 R. W. Ruhwandl and E. M. Terentjev, *Phys. Rev. E: Stat. Phys., Plasmas, Fluids, Relat. Interdiscip. Top.*, 1997, **55**, 2958–2961.
49 Q. K. Liu, Y. X. Cui, D. Gardner, X. Li, S. L. He and Smalyukh, II, *Nano Lett.*, 2010, **10**, 1347–1353.
50 J. S. Evans, C. N. Beier and I. I. Smalyukh, *J. Appl. Phys.*, 2011, **110**, 033535.
51 P. Yeh and C. Gu, *Optics of Liquid Crystal Displays*, John Wiley & Sons, Inc., 1999.

Electronic Supplementary Material (ESI) for Soft Matter

Liquid Crystals of Aqueous, Giant Graphene Oxide Flakes

Budhadipta Dan[a,d], Natnael Behabtu[b], Angel Martinez[d], Julian S. Evans[d], Dmitry V. Kosynkin[c], James M. Tour[c], Matteo Pasquali[b,c*], Ivan I. Smalyukh[d,e*]

SEM images of GGO flakes

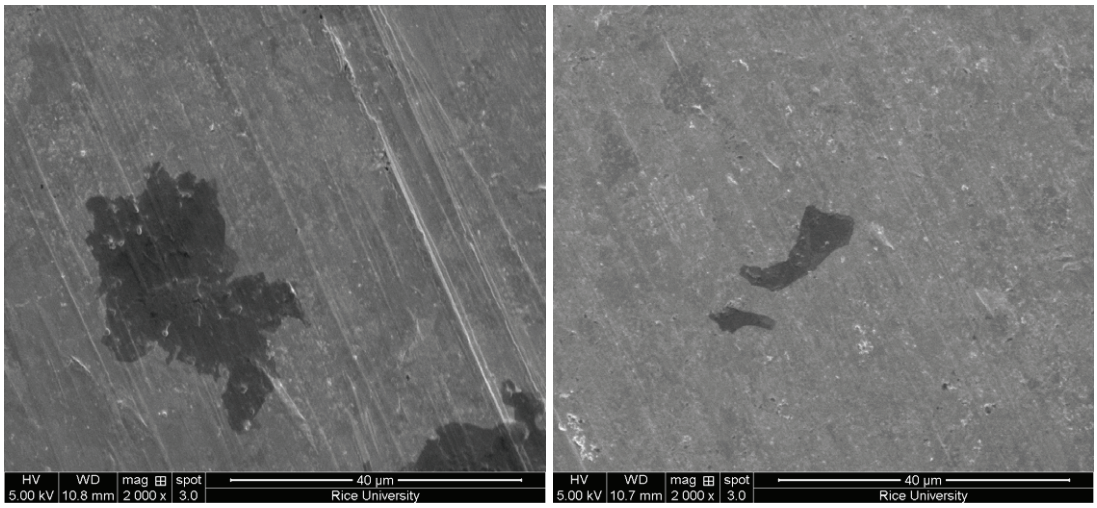

Figure S1: SEM image of GGO flakes showing their irregular, polygonal shape and presence of few ribbon-like structures.